Mechanisms of sliding friction studied with an array of industrial conical piezoelectric sensors

Gregory C. McLaskey and Steven D. Glaser
Department of Civil and Environmental Engineering, University of California, Berkeley, USA

ABSTRACT

We use a new design of high-fidelity nanoseismic sensors to detect the stress waves produced at the initiation of sliding during stick-slip friction. The piezoelectric sensors can detect radiated waves just a few pm in amplitude in the frequency range of 10 kHz to over 2 MHz. The reported experiments are designed to provide insights that may be applicable to both fault scales and micro contact junctions. The sensors used are packaged in a hardened steel case to facilitate their use in the field. The transducer's small size (14 mm threaded body, 30 mm long) permits a dense population of sensors to be installed on laboratory-sized samples, or surrounding localized centers of damage on structural applications. The closely spaced sensor array facilitates the localization of individual load releases from tiny asperities on a cm-scale frictional interface. At the same time, the broadband response of the conical piezoelectric sensors makes possible the study of source dynamics using theory developed for the study of earthquake source mechanisms via radiated seismic waves.

Keywords: multi-contact interface, stick slip, acoustic emission, stress wave propagation, fault rupture

1. INTRODUCTION

Under different conditions, sliding between two nominally flat surfaces may occur as a creeping motion, stick-slip phenomena, or some combination of the two. While these types of phenomena are widely observed and can be described empirically (e.g. rate- and state-dependent friction laws), the mechanisms responsible for this complicated behavior are still poorly understood. During the rapid transition from stick to slip, the force of friction which resists shear motion between the two surfaces is suddenly released or reduced. If this reorganization of tractions on the surfaces is rapid enough, it will cause stress waves to radiate away from the frictional interface and propagate throughout the bulk of the material. When the frictional interface is a km sized fault in the earth, this phenomena is known as an earthquake, but similar behavior has been observed on laboratory-sized faults[1-6].

In our current work, we study the mechanisms of friction, particularly the transition from stick to slip, via the stress waves (sounds) which are radiated from the frictional interface in much the same way seismologists study faulting via seismic waves. One goal of this research is to try and distinguish between different types or modes of rupture which may occur during the transition from stick to slip (i.e. crack like or pulse-type rupture[7] versus creeping behavior[8]). Another goal is to link particular rupture mechanisms with the type of seismicity they produce. For example, some faults in the earth are known to slip "silently"; they slip continuously or episodically without producing earthquakes[9]. Other faults produce devastating earthquakes which can inflict millions of dollars in property damages. It is hoped that insights gained in the laboratory which link responsible mechanisms to radiated stress waves may be applied to the advancement of understanding of processes occurring on the fault scale.

For this work, we employ an array of extremely sensitive, absolutely calibrated sensors to detect the high frequency displacements caused by the stress waves. The piezoelectric sensors, to be produced industrially, can detect radiated waves down to a few pm in amplitude in the frequency range of 10 kHz to over 2 MHz. These sensors will henceforth be referred to as nanoseismic sensors due their analogous role to that of seismic instruments and the extremely small amplitude and high frequency displacements they are capable of recording.

Section 2 presents a simplified view of micro-scale roughness of nominally flat surfaces and a basic description of the material interaction at the interface between a sliding block and a base plate. Section 3 describes some of the common experimental methods used to study this frictional behavior including currently practiced acoustic methods as well as the

methods of this study. A detailed description of the sensors used in this study is given in Section 4. Experimental methods and typical results from preliminary experiments are presented in Section 5.

2. THE SLIDING BLOCK PROBLEM

A basic description of the experimental setup is shown in Figure 1. As shown, a slider block is pressed onto a base plate with a normal force F_n and pushed in the x direction with a shear force F_s through a spring of stiffness k.

Modern studies of surface topography have revealed that a surface which appears nominally flat on the mm and cm scale is in almost all cases quite rough on the μm scale[10]. When two nominally flat surfaces are brought together, this micro-scale roughness or topography causes the surfaces to only interact at the highest peaks, sometimes known as junctions. A diagram depicting this interaction is shown in Figure 1 (b). Note that the scale of the surface roughness in the z direction is greatly exaggerated.

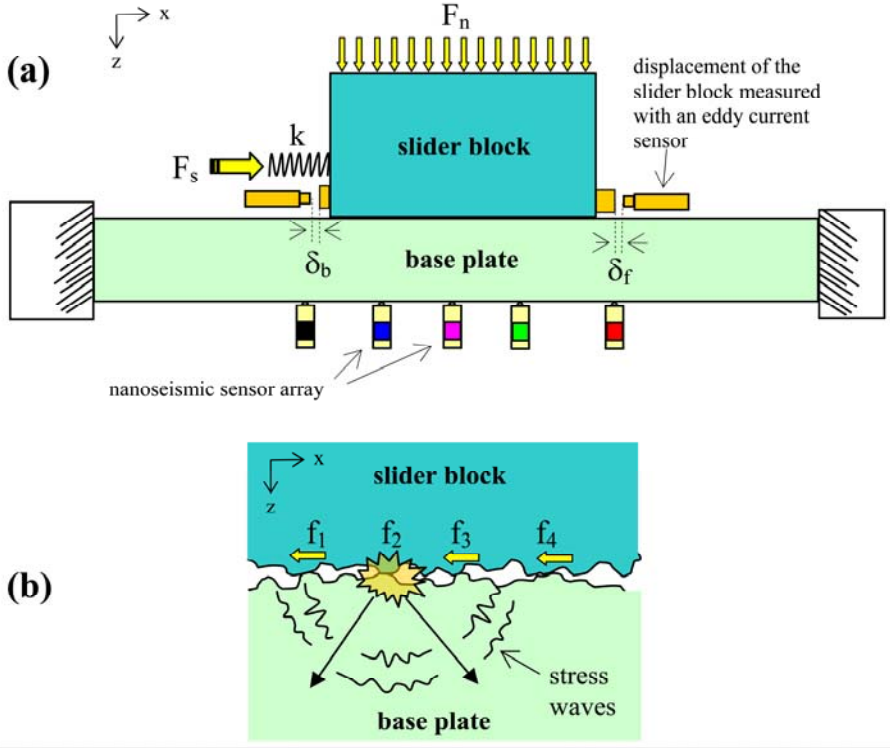

Figure 1: The basic experimental configuration for the sliding block experiment (a). Due to micro-scale roughness of the surfaces, the slider and base plate only interact at tiny junctions (b). In typical experiments of this type, a normal load F_n and a shear load F_s are applied, and the global displacement of the block is measured. The current experimental setup employs an array of very sensitive nanoseismic sensors that can detect high frequency displacements which are the result of stress waves radiated from the frictional interface (similar to earthquakes).

A normal force applied to the slider block will initially be carried by a population of relatively few junctions, each with a small area of contact (only the highest peaks will be in contact). In many cases the stress on these few junctions will exceed the yield stress of the material and cause plastic deformation[11,8]. This, as well as accompanying elastic deformation, will cause the highest peaks of the surface to be flattened and compressed which will allow the next-highest peaks to begin to interact and carry some of the normal force. Eventually, the total area of all junctions will be large enough to carry the full normal load F_n without any further yielding. The total contact area of all interacting junctions is known as the true area of contact Σ_t, and it is typically much smaller than the nominal area of contact Σ_n which would be calculated assuming the macroscopic geometry of the nominally flat surfaces.

The junctions also carry the shear load on the slider block. For a wide range of materials and surface roughness, the shear load that the junctions can carry is directly proportional to the true area of contact Σ_t. The well known

observation that the shear force $F_s = \mu F_n$ (where μ is the friction coefficient) is due to the fact that the true area of contact is directly proportional to the normal force and not dependent upon the nominal area of contact Σ_n.

The total shear force Fs is resisted by the sum of the shear forces on each of the n individual junctions which constitute the entire multi-contact interface (i.e. $F_s = \sum_{i=1}^{n} f_i$). This process is depicted in Figure 1 (b). If the local load carried by one of the junctions (f_2 in the figure) becomes too great and is suddenly released, either from sudden slip or breaking of the junction, the resulting local redistribution of stress on the interface will cause stress waves to radiate away from the interface (earthquake waves in the case of a fault). These waves will cause displacements which can be recorded with an array of sensors (shown in Figure 1 (a)), located some distance away from the interface. The redistribution of stress may cause neighboring junctions to fail which may cause other junctions to fail which may eventually cascade into gross sliding of the whole block relative to the base plate.

3. EXPERIMENTAL SRATEGIES

The study of friction is particularly difficult due to the extremely broad range of scales involved, both in space and time. Temporally, things occur both very rapidly and very slowly. For example, crack-like ruptures with extremely large stresses near the crack tip may propagate close to the speed of sound in the material (around 1-10 km/s) while typical loading rates for shear experiments are on the order of μm/s. Spatially, a frictional interface may extend many cm while micro-scale roughness may interact to form contacts on the μm scale. This wide range of scales presents serious challenges both with modeling and with experimental observations.

A great deal of friction research has been performed using the sliding block experiment shown in Figure 1. Typically, the rigid body displacement of the block and the normal and shear loads are recorded as a function of time. In some experiments, the block is slowly loaded until sliding commences. In other experiments, the sliding and normal load are kept constant and the required shear load is recorded as a function of velocity and time. The first type of experiment is, at first glance, similar to loading of faults during the earthquake cycle. The second type of experiment has produced a set of empirical relations known as the rate- and state- dependent friction laws[12,13] and these have been used as an analytical tool for the study of fault slip and friction[14]. These measurements and empirical laws are global or average measurements of the frictional interface, but they provide little insight into the micro mechanisms responsible for the observed global behavior such as junction formation and asperity interaction.

A few researchers have employed optical methods to learn more about the local processes involved with friction. Dieterich and Kilgore[15] have imaged micro-scale junctions in optically transparent materials and Rubinstein et al. [16] have used optical properties to map the dynamic changes in contact statistics which occur during and preceding the transition from stick to slip. Xia et al.[17] have used photo elasticity to study dynamic rupture propagation of a frictional interface. These experiments offer insights into material behavior for specific cases. Unfortunately, these types of methods are limited by low image acquisition rates (a few microseconds), and a difficult tradeoff between high resolution and a large field of view.

Many researchers have used acoustic methods to try and gain insights into the mechanisms of sliding friction[1-6]. In this type of experiment, sensors record the vibrations which results from stress waves radiated from the interface in much the same way as described in Section 1. The recorded signals will be a function of (1) the source characteristics such as the magnitude, direction, and rate of load release or redistribution (2) the wave propagation characteristics of the material, and (3) the sensor's instrument response function. The main finding of these studies is that acoustic/seismic activity measured on laboratory specimens, or "acoustic emission" as it is often termed, can be empirically correlated to parameters such as slip rate imposed in friction experiments, but the signals typically contain information that is extremely difficult to interpret.

The difficulty of data interpretation stems from (1) the low quality of the sensors (as compared to broad band instruments used in global seismic networks, for example) and (2) the extremely complicated propagation characteristics of the laboratory specimens. The result is that acoustic signals recorded from friction tests are typically not amenable to rigorous and quantitative analyses similar those performed on regional and global seismic records. Instead, acoustic emission analysis is confined to broad statistical measures such as emission rate and frequency size analyses, and few important insights into underlying physical processes have been made with this method.

In the present work, these two difficulties are overcome by (1) using absolutely calibrated broadband piezoelectric displacement sensors and (2) using a large, thick base plate as the propagation medium. Wave propagation solutions can be relatively easily calculated for this geometry. More details about the sensors and system calibration are presented in Section 4.

If the instrument response function and wave propagation characteristics are known, the characteristics of the source function can be found from inversion. For example, given a set of signals recorded from an array of sensors, the location of the source of the propagating waves can be found from the relative timing of wave arrivals via triangulation. The amplitudes and polarities of various wave arrivals will provide the information needed to determine the direction and orientation of the forces which produced the waves, and the shape, or time history, of a wave arrival will provide information about the rate of change of these forces. Thus, it is possible with this method to study the locations, directionality, and evolution of junctions and asperity interactions occurring on a tiny subset of the frictional interface.

4. SENSORS AND SYSTEM CALIBRATION

The sensors used in these experiments are a new industrial design of a conical piezoelectric sensor first developed by Proctor[18] and similar to those reported in[19,20]. The sensors are packaged in a hardened steel cylindrical case to facilitate their use in the field. The transducer's small size (14 mm diameter threaded body, 30 mm long) permits a dense population of sensors to be installed on laboratory-sized samples, or surrounding localized centers of damage on structural applications.

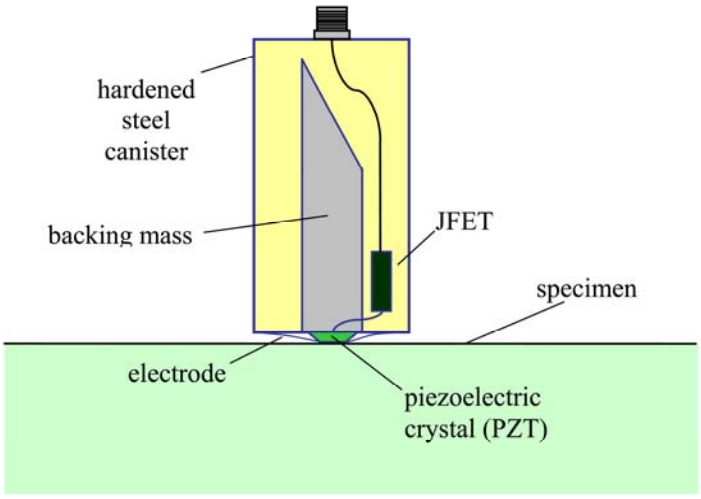

Figure 2. A schematic diagram of the sensor design. A piezoelectric crystal in the shape of a truncated cone is soldered to a backing mass which is potted in a hardened steel can with polyurethane rubber.

A basic diagram of the sensor design is depicted in Figure 2. The base of the truncated conical PZT-5a (lead-zirconium-titanate composition) sensing element is soldered to an irregularly shaped brass or lead backing mass which is potted in a hardened steel canister with polyurethane rubber. The sensor is mounted onto a specimen such that only the truncated tip of the conical piezoelectric element (covered by a thin nickel electrode) is in contact with the specimen. Normal displacements of the surface of the specimen will cause the PZT cone to be compressed between the surface of the specimen and the backing mass. This compression (or tension relative to the sensor's preload) will cause the PZT element to strain which will cause a measurable voltage between the two ends of the cone. This voltage is amplified with a JFET located inside the hardened steel canister to avoid signal loss due to parasitic capacitance.

The sensor is calibrated by comparing the recorded voltage output (signals) with the normal displacements which would be expected to occur (theoretically) in the absence of the sensor. The sensors were calibrated on the very same plates used for base plates for the friction experiments. Theoretical surface normal displacements are calculated by combining wave propagation solutions with known source functions. One form of the solution to the wave propagation problem is the Green's function. The advantage of the Green's function is that once the Green's function has been

calculated for a specific geometry, the waves which result from arbitrary loading can be found through convolution. Green's functions for the plates used in this study were calculated using generalized ray theory[21,22]. These Green's functions were validated with theoretical solutions[23-25] and finite element models[26].

Known source functions used for calibration experiments include (1) the sudden fracture of a thin walled glass capillary tube loaded on its side against the surface of the specimen, and (2) the impact of a tiny ball on the surface of the specimen. The sudden fracture of the glass capillary is known to present a force nearly equal to a step in time with a rise time of less than 200 ns[27]. The ball impact is known to produce an impulsive force on the surface of the material[28,29]. The duration of contact of the ball on the plate depends on the size and velocity of the ball as well as material properties, but is on the order of a few μs for ~ 1mm diameter balls at ~ 1 m/s incoming velocities. An example of a comparison between experiment and theory for a 0.40 mm diameter ruby ball dropped 325 mm onto a 50 mm polymethylmethacrylate (PMMA) plate is shown in Figure 3. For this experiment, the sensor is located 50 mm from the location of impact on the opposite face of the 50 mm thick plate. Theoretical displacements were calculated from a marriage between Hertz theory of impact (used to calculate the precise force time history that the ball imposes on the plate) and the elastodynamic Green's functions calculated for an infinite plate geometry using a generalized ray theory approach[21,22].

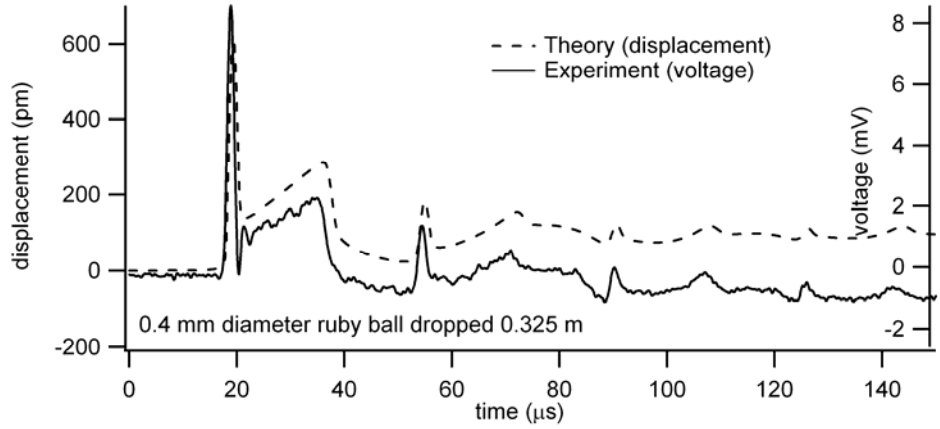

Figure 3. The time series of the sensor output (experiment) and surface normal displacements (theory) due to a 0.4 mm diameter ruby ball dropped 0.325 m onto a 50 mm thick PMMA plate (from McLaskey and Glaser[30]).

Resonant behavior in typical piezoelectric sensors will distort the recorded displacements. As shown in Figure 3, resonant behavior in these sensors is minimized and every wave arrival can be clearly identified, even the picometer amplitude arrivals which arrive in the "coda" of the signal due to multiple reflections through the thickness of the PMMA plate. This level of agreement between theory and experiment was previously not possible. The piezoelectric sensors can detect surface displacements just a few pm in amplitude in the frequency range of 10 kHz to over 2 MHz. A detailed description of the calibration procedures can be found elsewhere[30].

5. EXPERIMENTS AND PRELIMINARY RESULTS

A series of sliding block tests is currently being conducted using PMMA slider blocks and base plates. The experimental configuration is similar to that depicted in Figure 1 (a). A planar array of 12-14 nanoseismic sensors is located underneath the base plate. In a typical experiment, the slider block (dimensions 120 mm by 12 mm by 50 mm in the x, y, and z directions, respectively) is loaded with a normal load of about 300 N against a thick PMMA base plate (27 mm thick and 400 mm square, and then loaded in shear until slip occurs.

PMMA was chosen for both the slider and base materials because of its wave propagation properties. For most wave propagation problems, PMMA is well modeled as a linear elastic homogeneous material, but stress waves above about 50 kHz propagating through this material will be highly attenuated after they have propagated no more than a few hundreds of mm. This attenuation is great enough that all high frequency wave arrivals (greater than 50 kHz) felt by the sensors can be assumed to be direct arrivals from the frictional interface or nearby region, and wave propagation solutions for infinite plate geometry can be used for analysis procedures. This keeps the wave field free from high

frequency reflections from the outside edges of the plate and allows the easy identification of high-frequency, short-wavelength elastic wave arrivals.

During the experiment, the shear load is measured with a load cell, and the displacements of the front and back ends of the slider block relative to the base plate are measured with eddy current sensors. These quantities are recorded continuously at a sampling rate of 1 kHz. Simultaneously, the signals from the nanoseismic sensors are sampled at a rate of 10 MHz. When a signal from one of the nanoseismic channels meets the triggering criterion (e.g. it exceeds some threshold), the signals from all 16 channels (13 nanoseismic sensors, one load cell measuring the shear load, and two displacement sensors located on the front and back of the slider block) are recorded at a rate of 10 MHz for about 16 ms surrounding the time of triggering. In this way, a large time window is recorded at a low sampling rate, and a small time window surrounding a slip event is recorded at a higher sampling rate.

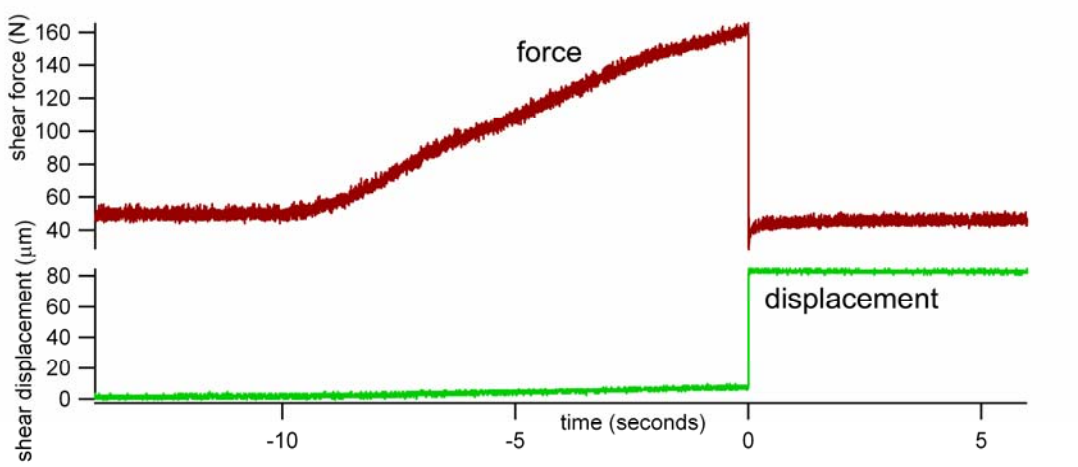

Figure 4. Shear load and displacement measured over a long time window at a reduced sampling rate show a sudden slip event.

In order to illustrate the analysis procedures possible with this experimental method and also to highlight some of the challenges, an example experiment is shown in Figures 4, 5, and 6, at different time scales. In this particular experiment, the rate of shear loading is relatively high (~10 N/s). As shown in Figure 4, the shear load is originally constant at about 50 N; then the shear load is increased at a roughly constant rate for ten seconds. During this loading stage, some shear displacement is observed due to compliance of the interface. At roughly time t = 0, the slider block slips (about 80 μm), and the shear load is rapidly reduced to the jamming level of about 50 N.

A closer examination of the loads and displacements near the time of slip is shown in Figure 5, and the sensor output from one of the nanoseismic sensors is shown in parallel. In this figure it is clear that the slip and corresponding load release is not instantaneous. Rather, the slider block slips for a duration of roughly 2 ms at a rate of roughly 40 mm/sec. The majority of the stress wave release occurs at the beginning of slip, though some high frequency waves are detected later, when the block is sliding and decelerating.

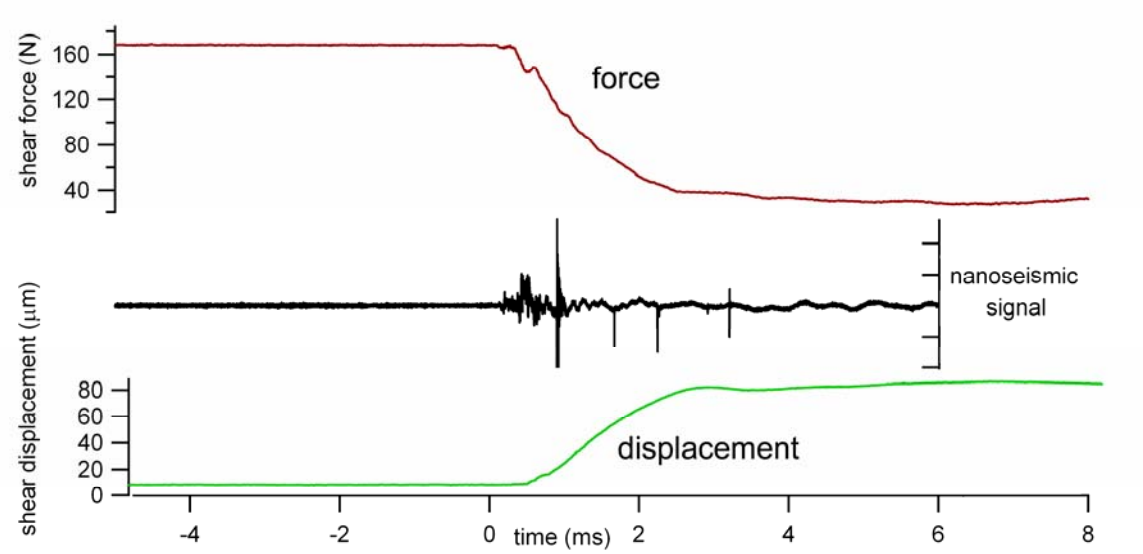

Figure 5: Signals from the same experiment shown in Figure 4 in a short time window surrounding the sudden slip event, recorded at a higher sampling rate (10 MHz). An example of a signal recorded by one sensor in the nanoseismic array is shown in parallel.

Figure 6 shows the initiation of sliding at even greater detail. The signals recorded from five different sensors in the nanoseismic sensor array are shown along with the shear load and displacement over the same time period. No change in either the shear load or displacement are detected until after a large stress wave release (at about 90 μs). This stress wave release was rapid enough that individual wave phases can be identified in the signals. For example, the signal recorded from sensor 1 (the thin solid black trace) shows a clear P-wave arrival followed by a larger amplitude S-wave arrival about 25 μs later. Another preliminary observation is that sensors located closer to the leading edge of the slider block than the location of first rupture show initial surface displacements in the negative z direction (see figure 1) while sensors located closer to the trailing edge show surface displacements in the positive z direction. Thus, sensors near the trailing edge see a compressional first arrival while sensors near the leading edge of the slider block see a dilatational first arrival.

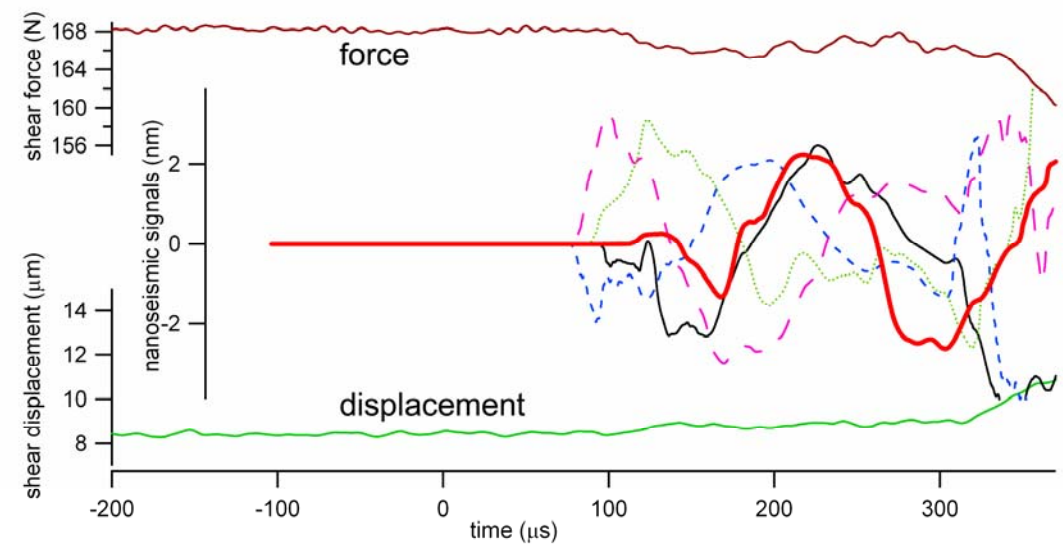

Figure 6: Signals from the same experiment shown in Figures 3 and 4 except at greater time and amplitude magnification. In this case the outputs from five different sensors in the nanoseismic array are shown.

It is much easier to analyze the signals recorded at the initiation of rupture than those later on in the rupture process because the first waves to arrive at the sensor locations are preceded by relative quiescence. For example, in the present

case, a second large wave reaches the sensor array at approximately 300-350 μs and is marked by a simultaneous drop in shear load and increase in displacement. This wave arrival is much more difficult to identify because the ~200 μs separation between the first main arrival and the second main arrival is not enough time for the waves in the plate to be sufficiently damped due to attenuation (internal friction) in the material.

The shape of this first wave pulse can give a good indication of the dynamics of first rupture. In the present case the first main wave arrival (at about 90 μs) shows a rise time of only a few μs. This implies that the main initial load release occurred in just a few μs time even when slip occurred for at least 2 ms.

6. CONCLUSIONS

This work demonstrates that the nanoseismic sensors described in this paper can be used as a tool to study details of sliding friction, especially at the initiation of sliding. Recorded signals are a function of the source, wave propagation effects, and instrument response functions. This complicated mixture of effects can cause signal interpretation to be extremely difficult. In the present work, the response function of the industrial conical piezoelectric sensors is known, and the propagation medium is a large, thick, homogeneous plate, for which wave propagation solutions can be attained. By including analysis procedures developed for observational seismology, we are able to establish a broader view of the processes involved in basic friction problems. Perhaps most importantly, we may be able to establish a relationship between seismicity (the production of stress waves) and underlying physical mechanisms. With proper scaling considerations, insights made in the laboratory may be scaled up to earthquake processes.

7. AKNOWLEDGEMENTS

This work was funded by NSF grant CMS-0624985.

8. REFERENCES

[1] Mair, K., Marone, C., Young, P. , “Rate Dependence of Acoustic Emissions Generated during Shear of Simulated Fault Gouge,” BSSA, 97, 6, 1841–1849 (2007).
[2] Sammonds, P., and M. Ohnaka. “Evolution of microseismicity during frictional sliding,” Geophys. Res. Lett. 25, 5, 699–702 (1998).
[3] Yabe, Y. , “Rate dependence of AE activity during frictional sliding”, Geophys. Res. Lett. 29, 10, 1388 (2002).
[4] Yabe, Y., N. Kato, K. Yamamoto, Hirasawa, T. “Effect of sliding rate on the activity of acoustic emission during stable sliding”, Pageoph 160, 1163–1189 (2003)
[5] Spetzler, H., G. Sobolev, A. Koltsov, A. Zang, and I. C. Getting, “Some properties of unstable slip on rough surfaces”, Pure Appl. Geophys. 137, 95 – 112. (1991)
[6] Voisin, C., J-R. Grasso, E. Larose, and F. Renard, “Evolution of seismic signals and slip patterns along subduction zones: Insights from a friction lab scale experiment”, Geophys. Res. Lett., 35, L08302. (2008)
[7] Heaton, T. “Evidence for and implications of self-healing pulses of slip in earthquake rupture”, Physics of the Earth and Planetary Interiors. 64 1-20. (1990)
[8] Bureau, L., Caroli, C., and Baumbeger, T. “Elasticity and the onset of frictional dissipation at a non-sliding multi-contact interface.” Proc. R. Soc. Lond. A. 459, 2787-2805. (2003)
[9] S. Ide, G. C. Beroza, D. R. Shelly, T. Uchide, “A scaling law for slow earthquakes”, Nature 447, 76 (2007)
[10] Persson, B.. [Sliding Friction]. Springer: Berlin. (1998)
[11] Bureau, L., Baumbeger, T., and Caroli, C., “Rheological aging and rejuvenation in solid friction contacts,” Eur. Phys. J. E. 8, 331-337 (2002)
[12] Dieterich, J. Modeling of Rock Friction 1. “Experimental Results and Constitutive Equations,” J. of Geophysical Research, 84 (B5) pp 2161-2168 (1979)
[13] Rice, J., and Ruina, A. “Stability of steady frictional slipping” J. Appl. Mech. 50 (2), pp 343-350 (1983)
[14] Marone, C. “Laboratory-derived friction laws and their application to seismic faulting,” Ann. Rev. Earth Planet. Sci. 26, 643–696 (1998).
[15] Dieterich, J. H., and Kilgore, B. D. “Direct observations of frictional contacts—new insights for state-dependent properties,” Pure Appl. Geophys. 143, no. 1–3 283–302. (1994)
[16] Rubinstein, S, Cohen, G., and Fineberg, J. “Detachment fronts and the onset of dynamic fricion,” Nature (London) 430, 1005. (2004).
[17] Xia, K, Rosakis, A., and Kanamori, H. “Laboratory earthquakes: the sub-Rayleigh-to-supershear rupture transition. Science 303, 1859 (2004).

[18] Proctor, T. M.. “An improved piezoelectric acoustic emission transducer,” J. of Acoustic Society of America. 71 1163-1168. (1982)
[19] Glaser, S., Weiss, G., and Johnson, L. “Body waves recorded inside an elastic half-space by an embedded, wideband velocity sensor.” Journal of Acoustic Society of America, 104, 1404-1412. (1998)
[20] McLaskey, G., Glaser, S. and Grosse, C., "Integrating Broad-Band High-Fidelity Acoustic Emission Sensors and Array Processing to Study Drying Shrinkage Cracking in Concrete," Proc. SPIE 6529, 65290C-4 (2007).
[21] Ceranoglu, A., & Pao, Y.. “Propagation of elastic pulses and acoustic emission in a plate.” Journal of Applied Mechanics: Transactions of the ASME 48 125-147 (1981).
[22] Helmberger, D. “Generalized ray theory for shear dislocations.” Bulletin of the Seismological Society of America. 64(1) 45-64 (1974).
[23] Knopoff, L.. “Surface motions of a thick plate.” J. of Applied Physics. 29(4) 661-670. (1958)
[24] Pekeris, C. L. “The Seismic Surface Pulse,” Proc. of the National Academy of Sciences 41, 469-480. (1955)
[25] Johnson, L.. “Green’s Function for Lamb’s Problem,” Geophys. J. R. astro. Soc. 37 99-131. (1974)
[26] McLaskey, G., Glaser, S., “High-fidelity conical piezoelectric transducers and finite element models utilized to quantify elastic waves generated from ball collisions,” Proc. SPIE, 7292, 72920S-1 - 72920S-18. (2009)
[27] Breckenridge, F., Tscheigg, C., and Greenspan, M. “Acoustic emission: some applications of Lamb’s Problem,” J. Acoustical Soc. Am. 57(3) 626-631 (1975)
[28] Goldsmith, W. [Impact], Dover Publications: New York. (2001)
[29] Johnson, K. [Contact Mechanics] Cambridge University Press, Cambridge (1985)
[30] McLaskey, G., Glaser, S., “Nanoseismic measurement of the localized initiation of sliding friction,” Proc. Batsheva de Rothschild Seminar on Shear Physics and the Meso-Scale in Earthquake and Landslide Mechanics, Ein Gedi, Israel, (2009).